ACS APPLIED ELECTRONIC MATERIALS

pubs.acs.org/acsaelm

Article

Straightforward Synthesis of Borophene Nanolayers for Enhanced NO_2 Detection in Humid Environments

Juan Casanova-Chafer* and Carla Bittencourt

Cite This: *ACS Appl. Electron. Mater.* 2025, 7, 2305−2312

Read Online

ACCESS | Metrics & More | Article Recommendations | Supporting Information

ABSTRACT: This study investigates the synthesis and gas sensing performance of borophene nanolayers produced through the sonochemical exfoliation method. The advantages of this method, including cost-effectiveness, simplicity and potential for scalability, make it a viable option for practical applications. High-resolution transmission electron microscopy (HRTEM) confirmed the successful exfoliation of boron into nanosheets with an average diameter of approximately 100 nm. X-ray diffraction (XRD) and X-ray photoelectron spectroscopy (XPS) analyses revealed the β-rhombohedral crystal structure. Additionally, the existence of carbon and oxygen on the surface has been determined and investigated. At room temperature, the borophene nanolayers showed exceptional gas sensing capabilities for detecting nitrogen dioxide (NO_2), especially in a humid environment. The sensitivity was significantly increased by about 50% when water molecules were present. These borophene nanolayers demonstrated unprecedented sensing performance for NO_2, with detection (LOD) and quantification (LOQ) limits of 23 and 76 ppb, respectively.

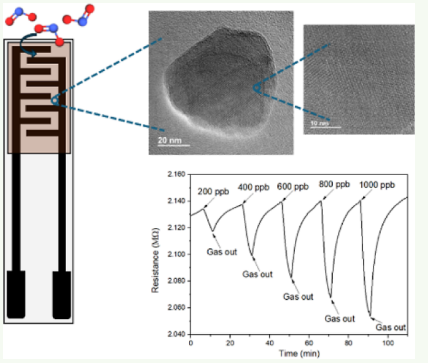

KEYWORDS: *borophene, chemical gas sensor, NO_2, sonochemical synthesis, humidity, ambient monitoring*

INTRODUCTION

Air pollution represents a critical societal challenge, significantly affecting human health and environmental quality, resulting in approximately 6.7 million premature deaths worldwide, as reported by the World Health Organization (WHO).[1] Consequently, there is an urgent need to monitor these contaminants to reduce exposure to hazardous levels.[2] Although established methods such as gas chromatography provide reliable and accurate measurements, their bulkiness, high cost, and impracticality for continuous monitoring pose significant challenges to the development of extensive sensing networks.[3] This has led to an increasing demand for cost-effective and miniaturized gas sensors capable of continuously monitoring air pollutants. Among the available technologies, chemical resistive (chemiresistive) sensors present a viable approach to building extensive sensing networks.[4−6] Such networks, characterized by a high density of measurement points, can effectively map pollution levels, providing valuable data to authorities for informed decisions to mitigate this exposure.

During the last years, most of investigations have focused on two-dimensional (2D) nanomaterials for gas sensing owing to their superior properties, including high surface-to-volume ratio and enhanced reactivity compared to their bulk counterparts.[7] Borophene, a 2D allotrope of boron, has recently attracted considerable research interest,[8] due to its unique electronic structure, which is characterized by high carrier mobility,[9] exceptional conductivity[10] and tunable bandgap,[11] indicating a high potential for gas sensor development. Furthermore, the excellent flexibility, elasticity, and strength of borophene enhance its applicability in flexible electronics.[12] In this perspective, borophene has been explored across various fields, including electrochemistry,[13] catalysis,[14] biosensors,[15] superconductivity[16] and photodetection.[17] However, despite numerous theoretical studies predicting its outstanding properties, empirical investigations into its potential for gas sensing remain limited.[18,19]

The method of borophene synthesis is critical for tailoring its properties for specific applications. Most research has employed molecular beam epitaxy (MBE), a technique known for yielding high-purity and high-crystallinity borophene layers.[20] However, this method is constrained by scalability issues, transfer step after the synthesis and cost-effectiveness. In contrast, sonochemical exfoliation presents a more practical alternative, offering a straightforward, economical, and scalable approach. This technique uses ultrasound waves to exfoliate bulk boron into 2D nanosheets, providing advantages in terms of cost and nanomaterial production. Although sonochemical exfoliation results in borophene with lower crystallinity than

Received: November 10, 2024
Revised: February 13, 2025
Accepted: February 14, 2025
Published: March 16, 2025

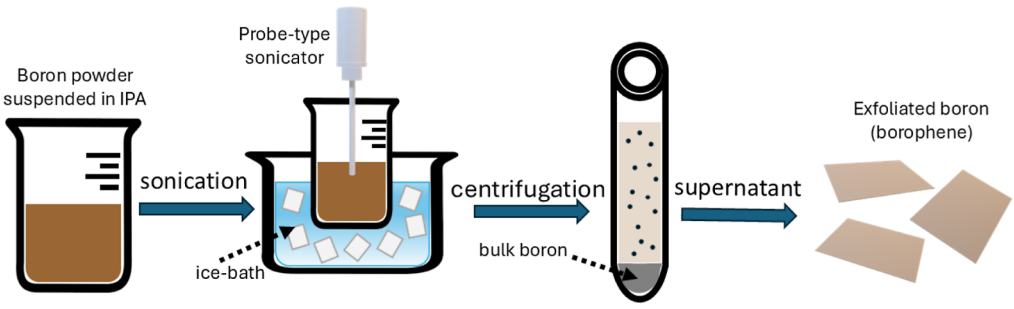

Figure 1. Schematic illustration of liquid-phase sonochemical exfoliation. Bulk powder was initially suspended in IPA and then sonicated using a probe-type sonicator. The resulting suspension was centrifuged to exfoliate the boron sheets and remove aggregates and bulk boron, which settled at the bottom of the centrifuge tube. Finally, the supernatant containing the borophene was collected.

MBE, this characteristic may not be detrimental to gas sensing performance. Surface defects and oxygen-containing groups formed during exfoliation could enhance the reactivity of borophene toward specific gaseous species.[21]

This study aims to demonstrate the potential of sonochemical exfoliation in producing borophene nanolayers with exceptional gas-sensing properties. The simplicity, cost-effectiveness, and scalability of this method make it particularly appealing for industrial applications and large-scale production. Specifically, this research focuses on detecting nitrogen dioxide (NO_2), a significant air pollutant with serious health effects, including respiratory illnesses, as well as environmental issues such as acid rain.[22]

EXPERIMENTAL SECTION

Borophene Synthesis. Commercially available pure boron powder with an average particle size of 2 μm and 2-propanol (IPA) was purchased from Merck. The sonochemistry method assisted with centrifugation applied in this work was adapted from the protocol synthesis proposed by H. Li and collaborators.[23] Figure 1 illustrates the different steps of the procedure. Initially, a suspension of boron in IPA (0.8 mg/mL) was prepared and subjected to an ultrasonic bath treatment for 5 min. Following this initial sonication, the suspension was immersed in an ice bath to maintain a stable temperature during the subsequent processing. A probe-type sonicator was employed, using pulsed ultrasonication (5 s intervals) for a total duration of 2 h. Meanwhile, the temperature of the ice bath was continuously monitored, and when it began to rise, ice was replaced to ensure stability and prevent solvent evaporation. To minimize contamination, this entire process was conducted in an airtight chamber.

After sonication, the supernatant was carefully collected and centrifuged at 6000 rpm for 15 min, a procedure that was repeated three times to eliminate any unexfoliated boron and aggregates. Due to the low concentration of the resultant nanomaterial, the borophene was dried at low temperature, weighed, and resuspended in IPA to achieve the desired concentration for subsequent application, such as deposition onto sensing electrodes or characterization of the nanomaterial.

Device Fabrication and Sensing Setup. The borophene suspension was deposited onto an alumina substrate using a spray pyrolysis method. Pure nitrogen served as the carrier gas for the deposition of borophene onto platinum screen-printed electrodes (Figure S1). Specifically, during the spray pyrolysis process, the hot plate was maintained at 120 °C, and the sprayer was positioned approximately 10 cm away from the device. The deposition procedure involved three cycles, each lasting around 20 s. Between cycles, a 1 min pause was applied at the programmed temperature to ensure complete removal of the solvent.

The obtained sensors were placed within an airtight Teflon chamber with a volume of 35 cm^3, connected to a gas mixing and delivery system. Sensing measurements were conducted in a pure dry air atmosphere (Air Premier purity: 99.999%) using calibrated gas cylinders containing NO_2 (1 ppm) diluted in dry air. A constant flow rate of 100 mL/min was maintained using mass-flow controllers (Bronkhorst High-Tech B.V.) and electronic valves. Additionally, a controlled evaporator mixer (Bronkhorst High-Tech B.V.) was used to introduce moisture into the atmosphere, enabling the assessment of the effects of humidity.

Before each gas exposure, the sensors were stabilized in dry air for 15 min. Each exposure to the target gas concentration lasted 5 min, with resistance changes continuously recorded using an Agilent HP 34972A multimeter. Finally, the sensor responses were calculated using the following equation

$$\text{Response}(\%) = (R_f - R_0)/R_0 = \Delta R/R_0 \times 100 \quad (1)$$

where ΔR represents the resistance change recorded during gas exposures, R_0 represents the baseline resistance in air, and R_f is the resistance recorded during the target gas exposure.

Characterization Techniques. The borophene layers were characterized using a high-resolution transmission electron microscope (HRTEM) operated at 200 kV (JEOL JEM 2100F). To prepare the sample, a few drops of the borophene suspension were deposited onto a lacy carbon film supported by a copper grid and left to dry at room temperature in a fume hood.

X-ray photoelectron spectroscopy (XPS) was conducted using a SPECS spectrometer equipped with a Phoibos 150 MCD-9 detector and a nonmonochromatic Al Kα (1486.6 eV) X-ray source. The spectra were recorded using an analyzer pass energy of 30 eV and an X-ray power of 100 W under a vacuum pressure of 10^{-9} mbar. The data analysis was performed using the CASA software. X-ray diffraction (XRD) patterns were recorded on a Philips X'PERT diffractometer equipped with a proportional detector and a secondary graphite monochromator. The data was collected stepwise over the range 2θ = 2−20° at steps of 0.02° at an accumulation time of 20 s/step and using the Cu Kα radiation (λ = 1.54178 Å).

RESULTS AND DISCUSSION

Nanomaterial Characterization. The physical and chemical properties of the synthesized borophene were thoroughly analyzed using various experimental techniques. HRTEM was employed to examine the morphological characteristics of the boron sheets. Figure 2a shows a typical obtained borophene sheet, which notably exhibits a reduced size with an average diameter of approximately a hundred nanometers. Figure 2b provides a magnified view, revealing the high crystallinity of the borophene, with an average interlayer distance of 4.9 Å. The inset in Figure 2b displays the fast Fourier transform (FFT) pattern, indicating the (104) plane of the β-rhombohedral structure.

Figure 3 depicts the XRD analysis, which reveals a B_{12} boron crystal structure. The diffraction pattern was indexed to the β-rhombohedral borophene crystal structure (JCPDS 00-031-0207), belonging to the $R\bar{3}m$ (no. 166) space group. This

https://doi.org/10.1021/acsaelm.4c02003
ACS Appl. Electron. Mater. 2025, 7, 2305−2312

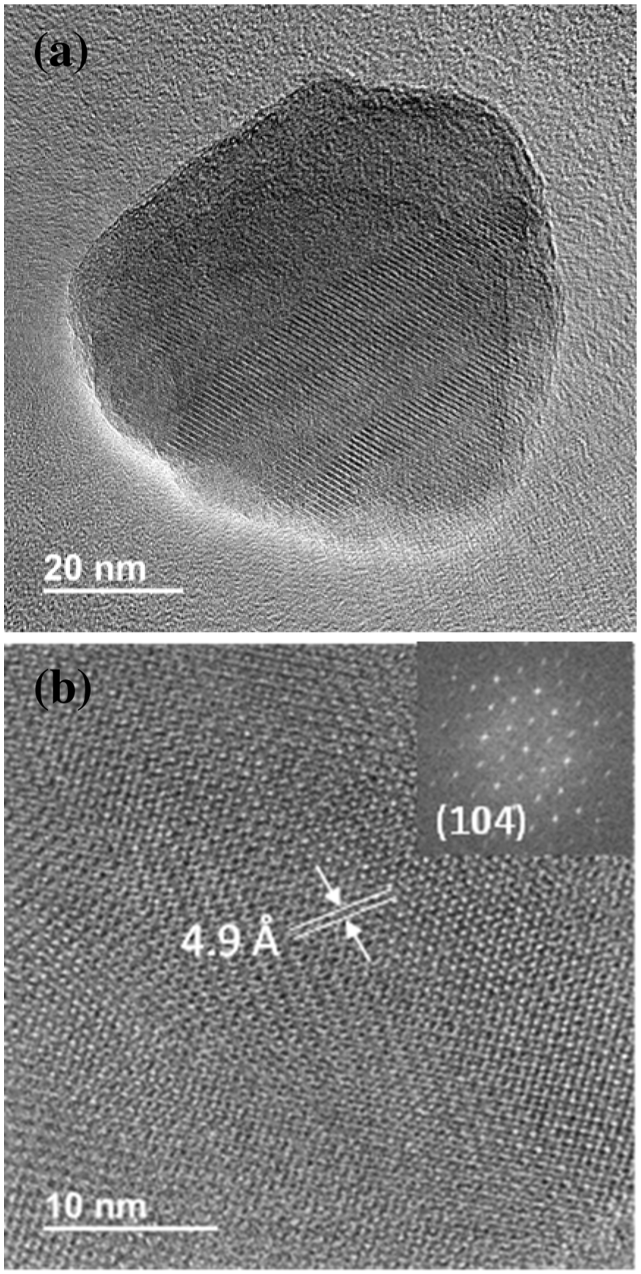

Figure 2. HRTEM images of borophene, (a) an overview of the nanolayer size, and (b) a higher magnification showing the high crystallinity and the interlayer distance. The inset shows the FFT pattern.

finding aligns with previous studies[13,24] and correlates with the structural parameters observed in the HRTEM analysis, suggesting that the proposed preparation method effectively retains the crystallinity of the bulk boron precursor.[24]

XPS was utilized to investigate the surface composition and chemical states of boron sonochemical exfoliation. Figure 4a displays the survey spectra, revealing peaks corresponding to B 1s, C 1s, O 1s, and N 1s, with atomic percentages (At %) of 48.9, 21.8, 27.5, and 1.8%, respectively. As expected, boron is the most abundant element, consistent with typical ranges reported in previous works.[23,24] However, the relatively high carbon and oxygen content is noteworthy, aligning with observations in those studies. These elements, along with the small amount of nitrogen, likely come from impurities

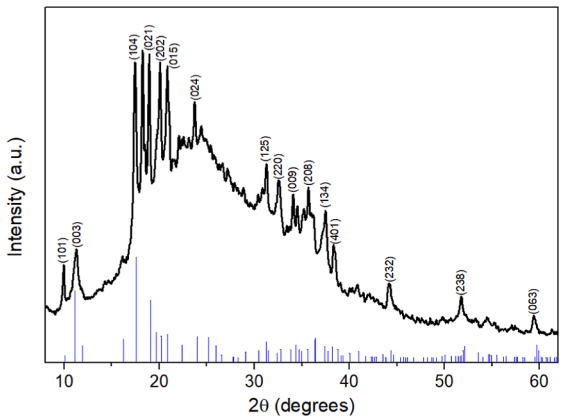

Figure 3. (a) XRD pattern of borophene with the JCPDS reference peaks.

introduced by the solvent during exfoliation and surface contamination upon exposure to air.[25] Due to the surface-sensitive nature of XPS, the presence of these elements is amplified. Nonetheless, the obtained borophene nanolayers exhibit greater stability and significantly reduced oxidation compared to other boron-based nanomaterials, such as 2H-Borophene, which shows a boron content of 17.3%.[26] Nevertheless, this drawback remains unresolved to date. The oxygen and carbon contents, coming upon air exposure and the use of solvents, also depend on the synthesis route followed. Some studies report up to 57% of oxygen for borophene samples.[27]

In this context, several approaches were explored to minimize the presence of oxygen. For instance, Liu et al. observed that borophene forms a superficial suboxide layer within 1 min of air exposure. But this issue could be avoided under ultrahigh vacuum (UHV) conditions.[28] While UHV effectively preserves borophene, it seems impractical for sensing applications. Similarly, Ranjan et al. demonstrated argon plasma etching as an effective method of reducing oxygen levels,[29] but the improvement would be temporary, as oxidation resumes upon re-exposure to air. Recent developments, such as borophane (hydrogenated borophene), aimed to increase its stability. Yet even borophane experiences oxidation by 6% in 1 h.[30]

In Figure 4b, the XPS high-resolution spectra for the B 1s core level showed three Gaussian−Lorentzian components centered at 187.6, 189.1, and 191.2 eV, corresponding to 69.0, 28.9, and 2.1% of the B 1s peak, respectively. The highest contribution to the B 1s peak is the component associated with B−B bonds in the β-phase structure, confirming the successful synthesis of borophene with minimal C and N-containing defects. However, the components at higher binding energies are associated with B−O bonds. Specifically, the peak at 189.1 eV corresponds to interstitial suboxide B_xO_y (x/y = 3),[31,32] which represents an initial stage of oxidation. This interstitial oxygen between the borophene nanolayers is likely introduced during the ultrasonication process from using IPA as a solvent.[33] Besides, the component with the lowest intensity, centered at 191.2 eV and constituting only about 2% of the signal, indicates the presence of a suboxide surface layer.[34] This second oxidation step, corresponding to suboxide B_xO_y ($1.5 < x/y < 3$),[31,33] have limited prevalence and could be attributed to the strong interaction between boron and oxygen. This is potentially due to the presence of coordinatively unsaturated

https://doi.org/10.1021/acsaelm.4c02003
ACS Appl. Electron. Mater. 2025, 7, 2305−2312

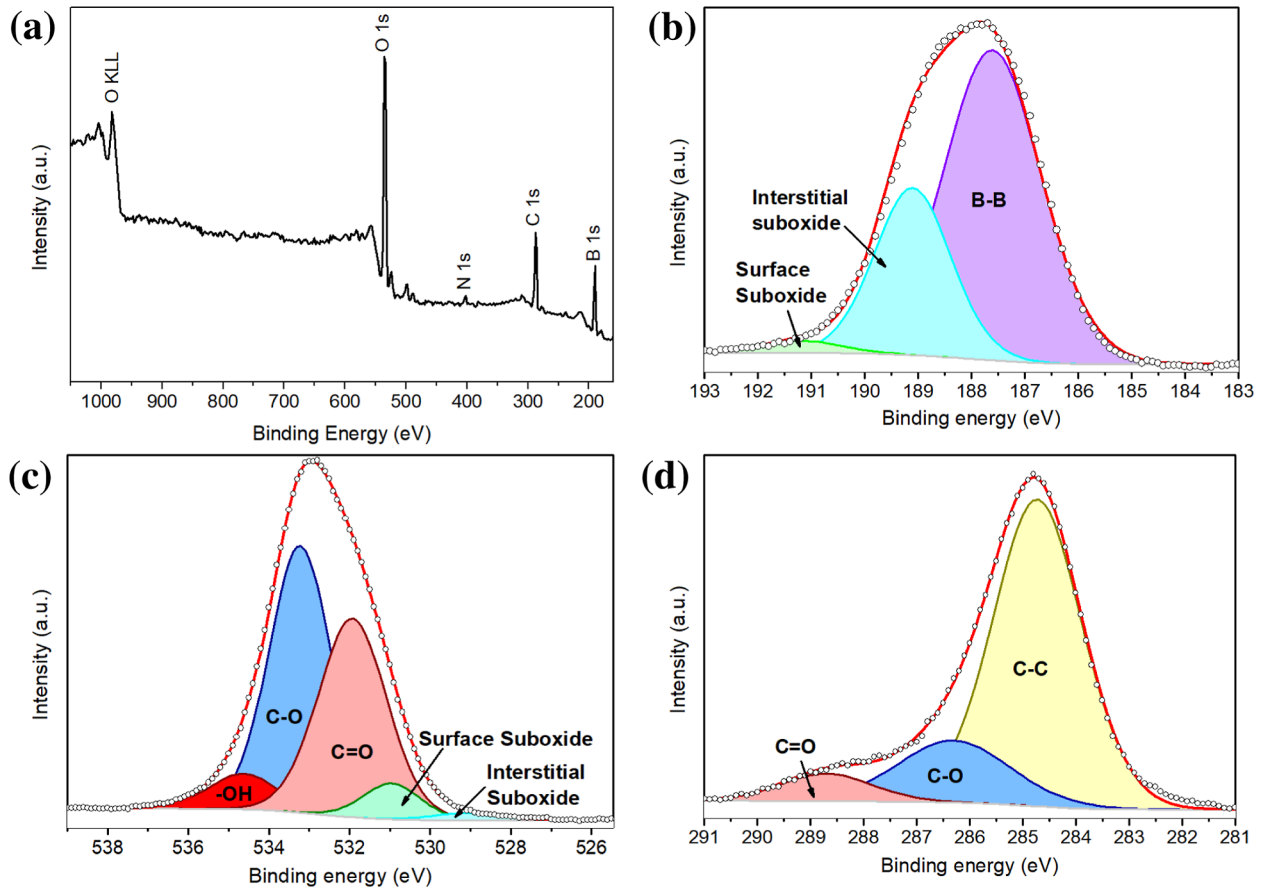

Figure 4. (a) XPS survey spectra showing elemental composition. XPS high-resolution spectra of (b) B 1s (c) O 1s and (d) C 1s core levels.

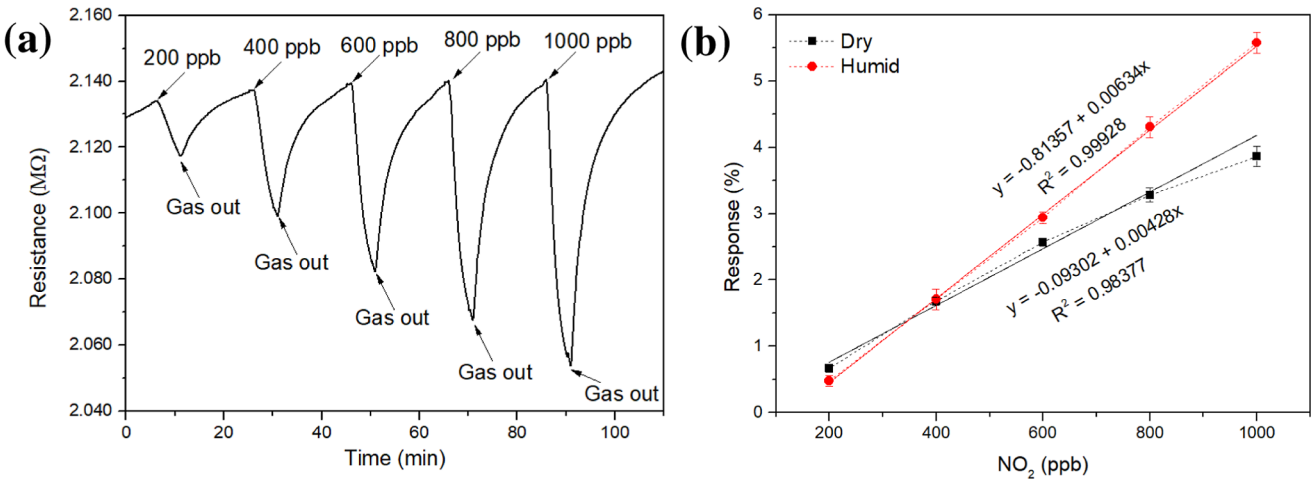

Figure 5. (a) Electrical response of borophene-based sensor to NO_2 detection within the 200−1000 ppb range at room temperature and under dry conditions. (b) Calibration curves (dashed lines) comparing NO_2 detection under dry and humid atmospheres (70% RH). The linear regression fittings (solid lines) are also shown, along with the corresponding linear regression equations and correlation coefficients.

boron atoms at the layer surface, likely resulting from a distorted edge effect.[35] This surface suboxide nanolayer is likely formed due to air exposure. However, it is worth noting that the borophene layers are not fully oxidized, which would otherwise result in the formation of B_2O_3 (x/y = 1.5). In the XPS spectra, this fully oxidized state would appear as a peak at a higher binding energy, around 192.4 eV.[36]

In Figure 4c, the O 1s spectrum was deconvoluted into five components to elucidate the nature of oxygen species present in the borophene sample. The peaks at lower binding energies are attributed to B−O bonds, specifically interstitial B_xO_y (x/y = 3) and surface B_xO_y (1.5 < x/y < 3) suboxides appearing at 529.1 and 530.9 eV, respectively. The peaks at 531.9 and 533.2 eV correspond to C═O and C−O bonds, respectively. These components are primarily associated with surface contamination from atmospheric exposure or solvent residues. Finally, the peak at 534.6 eV is attributed to hydroxyl groups (−OH) on the borophene surface.

https://doi.org/10.1021/acsaelm.4c02003
ACS Appl. Electron. Mater. 2025, 7, 2305−2312

Figure 4d illustrates the XPS high-resolution spectra for the C 1s peak, which can be deconvoluted into four distinct components: C−C (284.8 eV), C−O (286.3 eV), and C═O (288.7 eV), corresponding to atomic percentages of 74.3, 18.9, and 6.8, respectively. The C−C bonds detected, as well as those involving carbon and oxygen, are likely from surface contamination due to atmospheric exposure.

Gas Sensing Studies. The ability of borophene to detect NO_2 in the ppb concentration range was evaluated. Initial tests involved multiple cycles of increasing NO_2 concentrations (200, 400, 600, 800, and 1000 ppb) under a dry atmosphere at room temperature. An example of the electrical responses is illustrated in Figure 5a, revealing the remarkable sensing performance, including dynamic recovery of the baseline resistance and an exceptional signal-to-noise ratio. Besides, Figure S2a reveals a noteworthy repeatability. Based on these promising results, further experiments were conducted under a humid atmosphere, with 70% relative humidity (RH), an essential condition for practical applications. Figure S2b depicts the resistance changes under high RH, indicating that the device still maintains remarkable resistance recovery and stability.

Nevertheless, it should be noted that over extended measurement periods, a slight baseline drift can be observed. While repeatability was not compromised during the conducted experiments, this drawback should be considered for prolonged sensor operation. In this context, strategies such as sensor heating or UV irradiation for a few minutes could serve as effective methods to fully desorb gas molecules from the sensor surface and recover the original baseline level.

Figure 5b compares the calibration curves for NO_2 detection under dry and humid conditions. The presence of water molecules significantly enhances the sensor performance, resulting in greater resistance changes and increased sensitivity (as indicated by the steeper slope). This highlights the superior capabilities of borophene sensors in humid environments. Besides, it is worth noting that the enhancement effect of ambient moisture on the response to NO_2 becomes more pronounced as the analyte concentration increases.

To evaluate the potential for real-world applications, the limit of detection (LOD) and limit of quantification (LOQ) were calculated using the following formulas

$$\mathrm{LOD} = 3\frac{S_y}{b} \tag{2}$$

$$\mathrm{LOQ} = 10\frac{S_y}{b} \tag{3}$$

where S_y represents the standard deviation of the y-residuals, and b is the sensitivity (slope) from the calibration curves. Table 1 summarizes the results, highlighting that detection limits were achieved in the low ppb range.

Notably, the sensor performs significantly better in humid conditions, making it more suitable for practical scenarios where humidity is prevalent. Dry environments are mainly limited to lab conditions, whereas real-world settings tend to have significant humidity. Under humid conditions, the limits for NO_2 are approximately four times lower than in dry conditions. The LOD and LOQ achieved in humid conditions are well below the threshold limit values (TLV) established by European Air Quality Standards for safe breathing in the 27 EU countries. The 1 h NO_2 exposure limit is set at 200 $\mu g/m^3$ (resulting in 106 ppb).[37] Consequently, this borophene sensor can reliably detect (LOD = 23 ppb) and, more importantly, quantify (LOQ = 76 ppb) this air pollutant below the TLV.

Table 1. Limits of Detection (LOD) and Quantification (LOQ) for NO_2 Sensing under Dry and Humid Conditions

	dry atm.	humid atm.
LOD (ppb)	99.5	22.8
LOQ (ppb)	331.8	75.9

Table 2 presents a comparative analysis of the performance of bare borophene devices and heterostructures using this nanomaterial, specifically focusing on NO_2 detection at room temperature. Several significant observations can be drawn from this table, indicating that this study reports the highest sensitivity coefficient and the smallest borophene sheet diameter. These two parameters are likely interrelated, as reduced sheet size increases the surface area-to-volume ratio, resulting in a higher edge density that introduces more defects and impurities. Such features likely function as reactive sites for gas molecules. Moreover, when evaluating the synthesis method used to obtain borophene, this work demonstrates several-fold improvements in sensitivity compared to prior studies using a sonochemical protocol. Notably, the LOD achieved in this study is nearly 10 times lower than those previously reported values for NO_2 detection using borophene.

The exfoliated boron sheets suspended in IPA solution exhibited remarkable stability over time, remaining free from agglomeration. However, it is important to note that a superficial suboxide layer may form upon the deposition of borophene. Additionally, the presence of oxygen and carbon impurities originating from solvents and air contamination is relatively significant. While these carbonaceous and oxygen species may adversely affect other applications, such as photovoltaic devices, they can enhance gas sensing performance by acting as active surface sites that facilitate interactions with target gases. Furthermore, given that reactive sites and defects are probably located at the edges of the borophene layers, considering that nanolayers are obtained, a high density of active sites for gas interactions is expected, resulting in unprecedented sensitivity using bare borophene.

Considering the results summarized in Table 2, it is worth highlighting that, to date, reported borophene-based gas sensors have focused on room-temperature operation. This approach reveals their potential as inexpensive and low-power-consumption sensing devices, making them more attractive for practical applications. However, a promising avenue for future research can be based on investigating the effects of higher operating temperatures, particularly under humid conditions. Such studies could provide deeper insights into the interplay between temperature, humidity, and gas sensing mechanisms in borophene-based sensors, potentially optimizing the sensing performance further.

The potential selectivity of borophene was assessed by testing its response to other possible interfering gases, such as CO_2 and benzene (C_6H_6) under humid conditions. Figure S3 shows no significant interactions for these gases, as evidenced by the lack of observable resistance changes. This behavior aligns with theoretical predictions available in the literature. Density Functional Theory (DFT) calculations indicate that NO_2 chemisorbs strongly onto the borophene surface, with a high binding energy of 2.32 eV and significant charge transfer (−0.72 e).[38] In contrast, CO_2 and benzene tend to interact

https://doi.org/10.1021/acsaelm.4c02003
ACS Appl. Electron. Mater. 2025, 7, 2305−2312

Table 2. Comparison of NO_2 Sensing Performance at Room Temperature Using Various Borophene-Based Sensors[a]

nanomaterial	synthesis method	sheet diameter (≈nm)	response (%)/concentration (ppm)	sensitivity coefficient (%/ppm)	LOD (ppb)	reference
Ba-borophene	sonochemical	N/A	51.5/25	2.1	N/A	45
Borophene-PEI-ZIF-8	sonochemical	200	24.1/25	0.96	N/A	43
Borophene	CVD	N/A	422/100	4.22	200	42
Borophene	sonochemical	100	5.6/1	5.6	22.8	this work

[a]N/A: data not available.

weakly with borophene through physisorption.[39] For instance, benzene exhibits negligible charge transfer (+0.01 e) when interacting with the borophene surface.[40] These findings reveal that borophene-based gas sensors hold substantial promise for the selective detection of NO_2, with minimal interference from other gas species.

Sensing Mechanisms. Despite theoretical predictions suggesting that borophene should exhibit metallic behavior,[41] experimental observations indicate that it behaves as a p-type semiconductor.[42] This phenomenon is likely attributable to the presence of defects and bonding with oxygen and carbon, leading to holes (positive carriers) being the predominant charge carriers in this semiconductor type. The adsorption of NO_2, a strong oxidizing gas (electron-withdrawing), on the surface of borophene, reduces the resistance by increasing hole concentration. Additionally, the adsorption of NO_2 may lower the Schottky barrier, shifting the Fermi level closer to the valence band.[43] Experimental data confirm that negatively charged NO_2 molecules adsorbed on the borophene surface can be readily desorbed under pure airflow, releasing electrons and restoring the initial resistance of borophene. This behavior aligns with theoretical predictions, suggesting that NO_2 adsorption induces significant charge transfer, resulting in a pronounced electrical response while exhibiting moderate bonding energy, thereby facilitating desorption.[44]

Interestingly, the sensing performance for NO_2 is markedly enhanced in the presence of ambient moisture, consistent with previous reports.[42,45] Water molecules, similar to NO_2, function as electron acceptors at room temperature. This interaction likely produces an additive effect, where ambient moisture further amplifies NO_2 detection by increasing the concentration of positive charge within the borophene.[8]

However, it is worth noting that the sensor resistance baseline was higher in a humid atmosphere compared to dry conditions. Considering the sensor stabilization in the presence of humidity and without the target gas, the water molecules can replace adsorbed oxygen molecules on the semiconductor surface.[46] During this process, the desorbed oxygen molecules may release electrons back into the borophene. This electron release probably tends to reduce the hole concentration, leading to an increase in the baseline resistance. Besides, water molecules can form a surface adsorption layer, which can hinder charge carrier mobility,[47] contributing to the baseline resistance increase.

However, when NO_2 is introduced with a significant humidity content, its strong electron-accepting nature allows NO_2 to compete effectively with water molecules for surface sites. Thereby, NO_2 molecules can replace water molecules from the surface, potentially releasing charge transport pathways. This synergy can explain the enhanced sensor response to NO_2 in humid conditions, owing to more efficient interactions with the nanomaterial and amplifying the NO_2 responses in the presence of water molecules.

CONCLUSIONS

This study successfully demonstrates the efficacy of sonochemical exfoliation as a viable method for synthesizing borophene nanolayers with promising gas-sensing properties, particularly for the detection of NO_2 detection. The experimental results demonstrated high sensitivity to NO_2 at room temperature, indicating the potential for developing low-powered and durable gas sensors. Despite the presence of surface impurities such as oxygen and carbon, the stability of borophene and performance were not compromised. These impurities, likely located at the edges of the nanolayers, may enhance sensor behavior by increasing interaction with gaseous compounds. Furthermore, it is noteworthy that the sensing responses and sensitivity were significantly enhanced under humid conditions, achieving an LOD and LOQ of 23 and 76 ppb, respectively. Those NO_2 levels are well below regulatory thresholds. These findings highlight the potential of borophene as a highly sensitive nanomaterial, paving the way for developing low-power and efficient gas sensors.

ASSOCIATED CONTENT

Supporting Information

The Supporting Information is available free of charge at https://pubs.acs.org/doi/10.1021/acsaelm.4c02003.

Top and backside views of the gas sensing device; electrical responses of borophene to different concentrations of NO_2 under dry and humid conditions; sensor responses to potential interfering gases such as CO_2 and C_6H_6 (PDF)

AUTHOR INFORMATION

Corresponding Author

Juan Casanova-Chafer − *Chimie des Interactions Plasma-Surface (ChIPS), Chemistry Department, University of Mons, 7000 Mons, Belgium*; orcid.org/0000-0002-3508-3462; Email: juan.casanovachafer@umons.ac.be

Author

Carla Bittencourt − *Chimie des Interactions Plasma-Surface (ChIPS), Chemistry Department, University of Mons, 7000 Mons, Belgium*

Complete contact information is available at: https://pubs.acs.org/10.1021/acsaelm.4c02003

Funding

This research was funded by the Marie Skłodowska-Curie Individual Fellowship (Horizon Europe Program) under grant agreement No. 101066282 "GREBOS".

Notes

The authors declare no competing financial interest.

■ ACKNOWLEDGMENTS

We gratefully acknowledge Dr. Rocio Garcia-Aboal for her technical assistance in obtaining the HRTEM images and Dr. Pedro Atienzar for facilitating access to the HRTEM facility. Special thanks to Prof. Eduard Llobet for allowing us to use his sensing system. C.B. is a research associate of FNRS-Belgium.

■ REFERENCES

(1) Air quality, energy and health.
(2) Banga, I.; Paul, A.; Poudyal, D. C.; Muthukumar, S.; Prasad, S. Recent Advances in Gas Detection Methodologies with a Special Focus on Environmental Sensing and Health Monitoring Applications—A Critical Review. *ACS Sens.* **2023**, *8* (9), 3307−3319.
(3) Wang, L.; Cheng, Y.; Gopalan, S.; Luo, F.; Amreen, K.; Singh, R. K.; Goel, S.; Lin, Z.; Naidu, R. Review and Perspective: Gas Separation and Discrimination Technologies for Current Gas Sensors in Environmental Applications. *ACS Sens.* **2023**, *8* (4), 1373−1390.
(4) Chiu, S. W.; Tang, K. T. Towards a Chemiresistive Sensor-Integrated Electronic Nose: A Review. *Sensors* **2013**, *13* (10), 14214−14247.
(5) Elnabawy, H. M.; Casanova-Chafer, J.; Anis, B.; Fedawy, M.; Scardamaglia, M.; Bittencourt, C.; Khalil, A. S. G.; Llobet, E.; Vilanova, X. Wet Chemistry Route for the Decoration of Carbon Nanotubes with Iron Oxide Nanoparticles for Gas Sensing. *Beilstein J. Nanotechnol.* **2019**, *10* (1), 105−118.
(6) Mackin, C.; Schroeder, V.; Zurutuza, A.; Su, C.; Kong, J.; Swager, T. M.; Palacios, T. Chemiresistive Graphene Sensors for Ammonia Detection. *ACS Appl. Mater. Interfaces* **2018**, *10* (18), 16169−16176.
(7) Moumen, A.; Konar, R.; Zappa, D.; Teblum, E.; Perelshtein, I.; Lavi, R.; Ruthstein, S.; Nessim, G. D.; Comini, E. Robust Room-Temperature NO2 Sensors from Exfoliated 2D Few-Layered CVD-Grown Bulk Tungsten Di-Selenide (2H-WSe2). *ACS Appl. Mater. Interfaces* **2021**, *13* (3), 4316−4329.
(8) Mishra, R. K.; Sarkar, J.; Verma, K.; Chianella, I.; Goel, S.; Nezhad, H. Y. Borophene: A 2D Wonder Shaping the Future of Nanotechnology and Materials Science. *Nano Mater. Sci.* **2024**.
(9) Xu, J.; Chang, Y.; Gan, L.; Ma, Y.; Zhai, T.; Xu, J. Q.; Chang, Y. Y.; Gan, L.; Ma, Y.; Zhai, T. Y. Ultrathin Single-Crystalline Boron Nanosheets for Enhanced Electro-Optical Performances. *Advanced Science* **2015**, *2* (6), 1500023.
(10) Penev, E. S.; Kutana, A.; Yakobson, B. I. Can Two-Dimensional Boron Superconduct? *Nano Lett.* **2016**, *16* (4), 2522−2526.
(11) Wang, X.; Liang, J.; You, Q.; Zhu, J.; Fang, F.; Xiang, Y.; Song, J. Bandgap Engineering of Hydroxy-Functionalized Borophene for Superior Photo-Electrochemical Performance. *Angew. Chem., Int. Ed.* **2020**, *59* (52), 23559−23563.
(12) Hou, C.; Tai, G.; Liu, Y.; Liu, R.; Liang, X.; Wu, Z.; Wu, Z. Borophene Pressure Sensing for Electronic Skin and Human-Machine Interface. *Nano Energy* **2022**, *97*, 107189.
(13) Taşaltın, C.; Türkmen, T. A.; Taşaltın, N.; Karakuş, S. Highly Sensitive Non-Enzymatic Electrochemical Glucose Biosensor Based on PANI: B12 Borophene. *J. Mater. Sci.: Mater. Electron.* **2021**, *32* (8), 10750−10760.
(14) Lin, H.; Shi, H.; Wang, Z.; Mu, Y.; Li, S.; Zhao, J.; Guo, J.; Yang, B.; Wu, Z. S.; Liu, F. Scalable Production of Freestanding Few-Layer B12-Borophene Single Crystalline Sheets as Efficient Electrocatalysts for Lithium-Sulfur Batteries. *ACS Nano* **2021**, *15* (11), 17327−17336.
(15) Gupta, G. H.; Kadakia, S.; Agiwal, D.; Keshari, T.; Kumar, S. Borophene Nanomaterials: Synthesis and Applications in Biosensors. *Mater. Adv.* **2024**, *5* (5), 1803−1816.
(16) Zhang, Y.; Yuan, X.; Hao, J.; Xu, M.; Li, Y. Realizing High-Temperature Superconductivity in Borophene with Dirac States Assembled by Kagome and Honeycomb Boron Layers. *Mater. Today Phys.* **2023**, *35*, 101144.
(17) Wu, Z.; Tai, G.; Liu, R.; Hou, C.; Shao, W.; Liang, X.; Wu, Z. Van Der Waals Epitaxial Growth of Borophene on a Mica Substrate toward a High-Performance Photodetector. *ACS Appl. Mater. Interfaces* **2021**, *13* (27), 31808−31815.
(18) Ta, L. T.; Hamada, I.; Morikawa, Y.; Dinh, V. A. Adsorption of Toxic Gases on Borophene: Surface Deformation Links to Chemisorptions. *RSC Adv.* **2021**, *11* (30), 18279−18287.
(19) Shukla, V.; Wärnå, J.; Jena, N. K.; Grigoriev, A.; Ahuja, R. Toward the Realization of 2D Borophene Based Gas Sensor. *J. Phys. Chem. C* **2017**, *121* (48), 26869−26876.
(20) Li, W.; Wu, K.; Chen, L. Epitaxial Growth of Borophene on Substrates. *Prog. Surf. Sci.* **2023**, *98* (2), 100704.
(21) Yu, Z.; Li, Y.; Yu, X.; Chen, F. Computational Study of Borophene with Line Defects as Sensors for Nitrogen-Containing Gas Molecules. *ACS Appl. Nano Mater.* **2020**, *3* (10), 9961−9968.
(22) Worton, D. R. Future Adoption of Direct Measurement Techniques for Regulatory Measurements of Nitrogen Dioxide: Drivers and Challenges. *Environ. Sci. Technol.* **2020**, *54* (23), 14785−14786.
(23) Li, H.; Jing, L.; Liu, W.; Lin, J.; Tay, R. Y.; Tsang, S. H.; Teo, E. H. T. Scalable Production of Few-Layer Boron Sheets by Liquid-Phase Exfoliation and Their Superior Supercapacitive Performance. *ACS Nano* **2018**, *12* (2), 1262−1272.
(24) Zhang, F.; She, L.; Jia, C.; He, X.; Li, Q.; Sun, J.; Lei, Z.; Liu, Z. H. Few-Layer and Large Flake Size Borophene: Preparation with Solvothermal-Assisted Liquid Phase Exfoliation. *RSC Adv.* **2020**, *10* (46), 27532−27537.
(25) Wang, K.; Choyal, S.; Schultz, J. F.; McKenzie, J.; Li, L.; Liu, X.; Jiang, N. Borophene: Synthesis, Chemistry, and Electronic Properties. *ChemPlusChem* **2024**, *89*, No. e202400333.
(26) Tai, G.; Xu, M.; Hou, C.; Liu, R.; Liang, X.; Wu, Z. Borophene Nanosheets as High-Efficiency Catalysts for the Hydrogen Evolution Reaction. *ACS Appl. Mater. Interfaces* **2021**, *13* (51), 60987−60994.
(27) Wang, H.; An, D.; Wang, M.; Sun, L.; Li, Y.; Li, H.; Li, N.; Hu, S.; He, Y. B. Crystalline Borophene Quantum Dots and Their Derivative Boron Nanospheres. *Mater. Adv.* **2021**, *2* (10), 3269−3273.
(28) Liu, X.; Rahn, M. S.; Ruan, Q.; Yakobson, B. I.; Hersam, M. C. Probing Borophene Oxidation at the Atomic Scale. *Nanotechnology* **2022**, *33* (23), 235702.
(29) Ranjan, P.; Sahu, T. K.; Bhushan, R.; Yamijala, S. S. R. K. C.; Late, D. J.; Kumar, P.; Vinu, A. Freestanding Borophene and Its Hybrids. *Adv. Mater.* **2019**, *31* (27), 1900353.
(30) Wu, Z.; Tai, G.; Liu, R.; Hou, C.; Shao, W.; Liang, X.; Wu, Z. van der Waals Epitaxial Growth of Borophene on a Mica Substrate toward a High-Performance Photodetector. *ACS Appl. Mater. Interfaces* **2021**, *13*, 31808−31815.
(31) Moddeman, W. E.; Burke, A. R.; Bowling, W. C.; Foose, D. S. Surface Oxides of Boron and B12O2 as Determined by XPS. *Surf. Interface Anal.* **1989**, *14* (5), 224−232.
(32) Joshi, A.; Tomar, A. K.; Singh, G.; Sharma, R. K. Engineering Oxygen Defects in the Boron Nanosheet for Stabilizing Complex Bonding Structure: An Approach for High-Performance Supercapacitor. *Chem. Eng. J.* **2021**, *407*, 127122.
(33) Gu, Q.; Lin, H.; Si, C.; Wang, Z.; Wang, A.; Liu, F.; Li, B.; Yang, B. Tuning the Active Oxygen Species of Two-Dimensional Borophene Oxide toward Advanced Metal-Free Catalysis. *ACS Nano* **2024**, *18*, 30574−30583.
(34) Sielicki, K.; Maślana, K.; Chen, X.; Mijowska, E. Bottom up Approach of Metal Assisted Electrochemical Exfoliation of Boron towards Borophene. *Sci. Rep.* **2022**, *12* (1), 15683.
(35) Wang, L.; Xu, S. M.; Guan, S.; Qu, X.; Waterhouse, G. I. N.; He, S.; Zhou, S. Highly Efficient Photothermal Heating via Distorted Edge-Defects in Boron Quantum Dots. *J. Mater. Chem. B* **2020**, *8* (43), 9881−9887.
(36) Ong, C. W.; Huang, H.; Zheng, B.; Kwok, R. W. M.; Hui, Y. Y.; Lau, W. M. X-Ray Photoemission Spectroscopy of Nonmetallic Materials: Electronic Structures of Boron and BxOy. *J. Appl. Phys.* **2004**, *95* (7), 3527−3534.
(37) EU air quality standards—European Commission.

https://doi.org/10.1021/acsaelm.4c02003
ACS Appl. Electron. Mater. 2025, 7, 2305−2312

(38) Shukla, V.; Wärnå, J.; Jena, N. K.; Grigoriev, A.; Ahuja, R. Toward the Realization of 2D Borophene Based Gas Sensor. *J. Phys. Chem. C* **2017**, *121* (48), 26869−26876.
(39) Casanova-Chafer, J. Roadmap for Borophene Gas Sensors. *ACS Sens.* **2025**, *10*, 76−99.
(40) Sun, Q.; Yang, Z.; Huo, Y.; Liu, R.; Xu, L. C.; Xue, L.; Liu, X. Designing and Optimizing B1-Borophene Organic Gas Sensor: A Theoretical Study. *Surf. Sci.* **2022**, *719*, 122030.
(41) Peng, B.; Zhang, H.; Shao, H.; Xu, Y.; Zhang, R.; Zhu, H. The Electronic, Optical, and Thermodynamic Properties of Borophene from First-Principles Calculations. *J. Mater. Chem. C* **2016**, *4* (16), 3592−3598.
(42) Hou, C.; Tai, G.; Liu, Y.; Liu, X. Borophene Gas Sensor. *Nano Res.* **2022**, *15* (3), 2537−2544.
(43) Arkoti, N. K.; Pal, K. Improved Selectivity of Borophene Sensor towards NO2 Gas with PEI-ZIF-8 Overlayer. *Sens. Actuators, B* **2024**, *401*, 135033.
(44) Huang, C. S.; Murat, A.; Babar, V.; Montes, E.; Schwingenschlögl, U. Adsorption of the Gas Molecules NH3, NO, NO2, and CO on Borophene. *J. Phys. Chem. C* **2018**, *122* (26), 14665−14670.
(45) Arkoti, N. K.; Pal, K. Work Function Modification of Borophene by Barium Decoration Towards Room Temperature NO2 Gas Sensor. *Proceedings of IEEE Sensors*; IEEE, 2022.
(46) Huang, Y. H.; Yen, T. Y.; Shi, M. T.; Hung, Y. H.; Chen, W. T.; Wu, C. H.; Hung, K. M.; Lo, K. Y. Competition between Oxygen and Water Molecules on SiO2/P-Doped Si Surface: The Electrical Dipole Evolution on Water/Oxygen-Adsorbed Oxide Surface. *Sens. Actuators, B* **2023**, *376*, 133011.
(47) Zuo, G.; Linares, M.; Upreti, T.; Kemerink, M. General Rule for the Energy of Water-Induced Traps in Organic Semiconductors. *Nat. Mater.* **2019**, *18* (6), 588−593.

https://doi.org/10.1021/acsaelm.4c02003
ACS Appl. Electron. Mater. 2025, 7, 2305−2312